

NUMERICAL SIMULATIONS OF TEMPERATURE DYNAMICS DURING CW LASER IRRADIATION OF SILICON MICROSCALE STRIPS ON A DIELECTRIC SUBSTRATE

JIRI BERANEK^(1,2), NADEZHDA M. BULGAKOVA⁽¹⁾

⁽¹⁾HiLASE Centre, Institute of Physics of the Czech Academy of Sciences, Dolni Brezany, Czech Republic

⁽²⁾Czech Technical University, Faculty of Nuclear Sciences and Physical Engineering, Praha, Czech Republic

DOI: 10.17973/MMSJ.2019_12_2019100

beranekj@fzu.cz

The numerical model presented in this article describes the heating of a thin strip of amorphous silicon on glass substrate by a continuous-wave Ar⁺ laser. The heat flow equation is solved using a finite difference method based on the implicit scheme with splitting by coordinates. A short overview of the methods of numerical analysis is given and the finite difference method is described in details including the numerical scheme, the algorithms with discussion of their validity, the quality of approximation and stability. The results of the simulations with a high spatio-temporal resolution help to determine the exposure time necessary to melt the entire cross-section of silicon strip and to get insight into the final temperature distribution in silicon as well as in the glass substrate.

KEYWORDS

numerical modeling, heat flow equation, laser modification, amorphous silicon, melting, finite difference method, implicit scheme

1 INTRODUCTION

The theoretical analysis presented in this paper is related to processing of a material by continuous laser. This technique is well-established in industry as well as in laboratory practices [Nickel 2003]. In our case, the absorbing material is a thin strip of amorphous silicon (a-Si) on a SiO₂ substrate (fused silica glass). Continuous laser is focused on the a-Si and a part of its energy is absorbed, causing heating of the material above its melting point. When laser beam moves away from the molten part, material will cool down, crystallization will take place and a polycrystalline phase is observed in the processed material. Such laser micromachining has demonstrated a high quality of the processed a-Si strips in terms of crystallinity and optoelectronic properties [Franz 2019]. The typical scheme of the experiments is shown in Figure 1.

We present the numerical model of the dynamics of melting of a-Si strips for the experimental conditions [Franz 2019]. The numerical analysis requires solving the heat flow equation in the Cartesian coordinate system using a numerical grid with fine nanometric steps to reliably reproduce the laser-energy absorption depth and also a high temporal resolution to reproduce fast heating of top layers, which are subjected to

significant absorption of energy. To provide a general overview, the three main methods of numerical modeling are discussed, which are typically implemented when a numerical code tailored to a particular case is being developed, or which are at the heart of many commercial solvers. Further, we are describing in detail the implementation of one of them, the Finite Difference Method, and the features of solutions obtained by this method, in particular, its consistency, stability and accuracy are discussed.

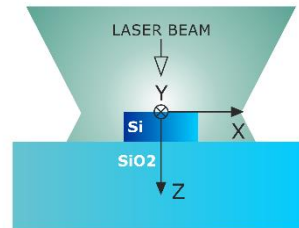


Figure 1. The typical scheme of experiments on laser processing of a-Si strips for waveguide applications. This scheme is considered in the present simulations, which were performed for the two-dimensional (x,z) case. The computational domain represents the cross section of a Si strip deposited on a fused silica substrate. X axis is parallel to the surface of the substrate and perpendicular to the strip orientation. Cw laser beam propagates along z-direction from the top, being focused on the surface of the Si strip. In the simulations presented in this paper, the Si strip is 0.4 μm thick (z dimension) and 2.1 μm wide (x dimension). The SiO₂ substrate is considered infinitely thick and infinitely wide. Its size in the simulations is sufficiently large to secure that the temperature at the remote boundaries remains undisturbed.

2 NUMERICAL SOLUTION OF THE HEAT FLOW EQUATION

Numerical mathematics and computation have been a subfield of mathematics throughout the history. In the past it was used as a tool only for the problems with a low computational cost as all the computations were done by hands. Now it is a well-established discipline that has spread into many fields so that its applications are often unified under the term computational science. As for the numerical analysis of partial differential equations (PDEs), the most important steps were taken in the beginning of 20th century and later they provided a basis for a significant development after the invention of the digital computers in mid of 1940s. Such problems were mainly dealing with technological problems arising from civil engineering and aerospace.

The heat flow equation is one of the canonical equations in physics, which expresses the conservation of energy within a medium with thermal conductivity k

$$\rho c_p \frac{\partial T}{\partial t} = \nabla \cdot k(\nabla T) + q. \quad (1)$$

Here T is the temperature, ρ is the density, c_p is the heat capacity of the considered system. If a system under investigation is supplied by an energy, the term q is nonzero. Construction of an analytical solution is possible in some cases and typically considerable simplifications are done even for a steady-state situation or when the conductivity of the material is isotropic and independent on temperature. In many practical problems, however, the simplifications required to make the system solvable analytically may lead to an incomplete picture of the process. In these cases, a numerical approach can give a description that produces reliable and useful results. Brief description of the most important numerical methods for solving PDEs is given in the next paragraphs.

2.1 Methods for solving PDEs

The main methods that are the key structural elements in the concept of numerical analysis of PDEs are the Finite Difference Method (FDM), the Finite Volume Method (FVM) and the Finite Element Method (FEM) (see, e.g., [Hoffman 1992, Mazumder 2015]). All the methods discretize the space to be computed (computational domain) and, in a specific way, they search for a solution that satisfies the initial equation(s). For the FDM, the computational domain is covered by a grid with a given spatial step in all directions. Using a particular difference scheme, the differentials in the equation are substituted by differences. Thus, a set of difference equations is obtained and an algorithm is used to look for an adequate solution that satisfies the initial equation(s). For obtaining the solution, the proper boundary conditions have to be applied at the boundaries of the computational domain. The FDM is a relatively straightforward method for obtaining a strong form solution, which means that we are solving a given equation in its original form.

In the FVM, the computational domain is discretized into the finite-sized volumes, which are connected to each other by vertices and edges or faces. The numerical values of a studied quantity belong to the center of each control volume. The FVM does not deal with the original equation, but uses the Gauss-Ostrogradski theorem (or divergence theorem) to integrate the equation over the volume of each element. The finite volume equation is then a balance condition for fluxes passing through the faces of these finite volumes and therefore the conservation property is at the heart of this method. As the equation is not in its original form, this form of solution is called the weak form.

Finally, the FEM discretizes the space in the convex elements. Similarly as in FVM, a weak (integral) form of the governing equation is found and the solution for each element is described as a linear combination of basic functions plus a test function (or error function), which is given by boundary conditions. Using a variational principle, the test function is minimized and a weak form of solution is found. This method was particularly successful for the problems in structural mechanics and the problems with complex geometries. Although it integrates the original PDE similarly to the case of the FVM, there is no guarantee that the conservation of a given quantity is insured. To address the problem of non-conservative nature, modifications of this method were developed.

2.2 The Finite Difference Method

For solving our problem of laser-induced melting of Si strips located on a SiO₂ substrate, we have chosen the FDM. Foundations of this method were first published in [Courant 1928]. Our problem does not possess any complex geometry and its governing PDE corresponds to a pure conservation of the thermal energy in a heat conductive media. Although the FVM may be a better candidate, we will clarify this choice by giving a more detailed description of the FDM applied to the time-marching calculation. Below it will be shown that the possible weak points of the FDM in comparison to the FVM can be compensated by using the backward-Euler method and a direct solver, which together mitigate some of possible sources of error and insure a good energy conservation.

The difference equation was derived using the central difference scheme for spatial derivative [Godunov 1987]. In this case, we have the second order accuracy scheme in space. Thus, the numerical error is reduced to one fourth when the grid spacing is halved and approaches zero when the Δx is further decreased. This is the mandatory condition of consistency of the difference

scheme. Error bound with approximation of time step is of first order. The final difference equation reads as

$$\rho c_p \frac{T_i^* - T_i}{\Delta t} = k \frac{T_{i-1} + T_{i+1} - 2T_i}{(\Delta x)^2}. \quad (2)$$

To find a solution T_i^* at a time moment $t = t_0 + \Delta t$, it is necessary to construct and solve a system of N linear equations. There are two ways of obtaining the unknown parameter at the new time moment, the explicit and implicit forms. The implementation of implicit method is more demanding as it requires to solve the system of all N equations together but, on the other hand, it offers unconditional stability. The explicit method is only stable when the following relation is satisfied.

$$\frac{\alpha \Delta t}{(\Delta x)^2} \leq \frac{1}{2}, \quad (3)$$

where $\alpha = k/\rho c_p$ is the thermal diffusivity and $\alpha \Delta t / (\Delta x)^2$ is called the grid Fourier number. The implicit form gives the relation

$$\xi = \frac{1}{1 + \frac{4\alpha \Delta t}{(\Delta x)^2} \sin^2 \frac{\theta}{2}}, \quad (4)$$

which is satisfied irrespective from the choice of Δx and Δt . Use of explicit method can lead to very small time steps and growth of computational cost of the simulation. Therefore, an implicit method is preferable for the studied problem, although its unconditional stability does not ensure physically meaningful result for all values of the time step because the accuracy can be significantly lowered by the truncation error [Mazumder 2015].

The solution itself can be split by the coordinates so that in one time step the directions are treated separately one after another [Godunov 1987]. Thus, the column-wise calculations are done firstly and row-wise solution is obtained in the second step. This has an advantage also in the choice of the solver because, for dense matrices of coefficients, iterative solvers typically have to be used to save time. Sparse or band matrices are solvable by direct methods without increasing drastically the computational time. Here, the Thomas algorithm is used to get exact solution of the system of equations.

Above, we have described the tools available for numerical solution of the heat flow equation over the computational domain space in time-advancing calculation. Below we report on application of the mathematical model to the real situation illustrated in Fig. 1.

3 IMPLEMENTATION AND MATHEMATICAL MODEL

Using the implicit method and taking the advantage of splitting by coordinates, we obtain two systems of linear equations given by equation (1) (note that we consider the temperature-dependent material parameters). By rearranging, we can write for x direction

$$\begin{aligned} -k_l T_{i-1}^* + \left(\frac{\Delta x^2}{dt} \rho c_p + k_r + k_l \right) T_i^* - k_r T_{i+1}^* \\ = \frac{\Delta x^2}{dt} \rho c_p T_i + q, \end{aligned} \quad (5)$$

where k_l and k_r are defined as

$$k_l = \frac{k_{i-1} + k_i}{2}, \quad k_r = \frac{k_{i+1} + k_i}{2}. \quad (6)$$

Here k_{i-1} , k_i and k_{i+1} are the thermal conductivities in the neighbouring cells $i-1, i$ and $i+1$ along x direction. The source term q is the energy supply to each cell given by the laser power P , laser beam radius r_0 , the reflection and absorption coefficients of the material, R and α respectively. Here, we assume the Gaussian profile of the laser beam which has the form

$$q(x, y, z) = (1 - R) \frac{2\alpha P}{\pi r_0^2} \exp\left(-\frac{x^2}{r_0^2} - \frac{y^2}{r_0^2}\right) \exp(-\alpha z), \quad (7)$$

For the z direction the identical equations are used but the source term of the laser energy is omitted as its contribution is already added at the considered time step:

$$\begin{aligned} & -k_u T_{i-n}^* + \left(\frac{\Delta z^2}{dt} \rho c_p + k_u + k_d\right) T_i^* - k_d T_{i+n}^* \\ & = \frac{\Delta z^2}{dt} \rho c_p T_i, \end{aligned} \quad (8)$$

where n is the number of cells in the direction x and k_u and k_d are defined as

$$k_u = \frac{k_{i-n} + k_i}{2}, \quad k_d = \frac{k_{i+n} + k_i}{2}. \quad (9)$$

These equations are written for each interior cell of the computational domain. For the cells on the boundaries, these equations are substituted by the boundary conditions. For the top, left and right boundary of the Si structure (Fig. 1), the condition of zero heat flux is applied as

$$k \frac{dT}{dx} \Big|_{xl} = 0, \quad k \frac{dT}{dx} \Big|_{xr} = 0, \quad k \frac{dT}{dz} \Big|_{zt} = 0. \quad (10)$$

Here xl, xr and zt denote the derivatives of x at the positions of the left boundary, the right boundary and z -derivative at the position of the top boundary respectively. The same condition holds for the part of the top boundary of SiO_2 substrate that is not contacting with the Si strip

$$k \frac{dT}{dz} \Big|_{zt} = 0, \quad (11)$$

where zt denotes the derivative at the top boundary of SiO_2 . Physically, this boundary condition states that no energy is leaving the Si and SiO_2 through these boundaries. The interface between Si and SiO_2 is the only one through which the heat can be transferred. The boundary condition at this interface is based on the conservation of energy, stating that

$$k \frac{dT}{dz} \Big|_{zt} = k \frac{dT}{dz} \Big|_{zb}. \quad (12)$$

Here zt and zb denotes the z -coordinate adjacent to the interface from the top (from Si strip) and the bottom (from glass side). The heat flux through the interface in both materials must be equal at the interface where both materials are in contact. Other boundaries of the substrate are considered to be sufficiently distant and do not influence the solution. Therefore these boundaries are shifting during the calculation in such a way that the computational domain of the substrate always contains the cells with the room temperature of 300 K.

To describe the melting process, we rewrite Eq. (1) to the following form [Zhvavyi 2006, Bulgakova 2010]

$$\left(\rho c_p + L_m \delta(T - T_m)\right) \frac{\partial T}{\partial t} = \nabla \cdot k(\nabla T) + q. \quad (13)$$

Here the term $L_m \delta(T - T_m)$ allows to follow the propagation of the liquid–solid interface during melting. T_m and L_m are the melting point and the latent heat of fusion respectively and the δ -function accounts for absorption of the fusion heat at the melting front.

3.1 Properties of the numerical solution

Each direction of calculations will give us one system of the linear algebraic equations given by the equations (5) and (8). The system of linear equations can be written in a matrix form as

$$\mathbf{M} T_i^* = T_i, \quad (14)$$

where \mathbf{M} is the square matrix with N rows and N columns and with all elements to be zeros except the three central diagonals. An example matrix for a simplified case where $N = 6$ looks as

$$\begin{pmatrix} f_1 & g_1 & 0 & 0 & 0 & 0 \\ e_2 & f_2 & g_2 & 0 & 0 & 0 \\ 0 & e_3 & f_3 & g_3 & 0 & 0 \\ 0 & 0 & e_4 & f_4 & g_4 & 0 \\ 0 & 0 & 0 & e_5 & f_5 & g_5 \\ 0 & 0 & 0 & 0 & e_6 & f_6 \end{pmatrix} \begin{pmatrix} T_1^* \\ T_2^* \\ T_3^* \\ T_4^* \\ T_5^* \\ T_6^* \end{pmatrix} = C \begin{pmatrix} T_1 \\ T_2 \\ T_3 \\ T_4 \\ T_5 \\ T_6 \end{pmatrix}, \quad (15)$$

where f_i are the coefficients of the central elements; e_i and g_i are the coefficients of the elements to its left and right respectively. The values of the tridiagonal matrix relate the outputs to the inputs and therefore have direct implications on the behavior of the mathematical model. This behavior is quantified by the condition number of matrix \mathbf{M} ,

$$\text{cond}(\mathbf{M}) = \|\mathbf{M}\| \|\mathbf{M}^{-1}\|. \quad (16)$$

The condition number for the well-conditioned matrix should be close to 1. The logarithm of the condition number tells how many decimal places are lost in one iteration. For our matrix, when the values of the coefficients are evaluated at the initial conditions using parameters shown in Table 1-3, we get $\text{cond}(\mathbf{M}) < 1.2$. Thus, our matrix can be considered as well-conditioned.

If the problem stated by our model has a solution, the solution is unique and changes continuously with the change of input parameters, then we call this problem well-posed. Our problem, the heat transfer with the given initial conditions, is a typical example of a well-posed problem. An example of the opposite situation, the ill-posed problem, is the inverse problem, when starting from the final state, the algorithm tries to find the initial temperature distribution.

The direct solution using the Thomas algorithm is a two-step process of forward elimination and backward substitution. The forward elimination removes the coefficients of the lower diagonal (Eq. (15))

$$f_i = f_i - \frac{e_i}{f_{i-1}} g_{i-1}, \quad (17)$$

$$r_i = r_i - \frac{e_i}{f_{i-1}} r_{i-1}, \quad (18)$$

$$e_i = 0, \quad (19)$$

where $i = 2, 3, 4, \dots$. The last equation for N^{th} cell has only one unknown value. The value for the coordinate x_N is evaluated and substituted into the equation for x_{N-1} and the process is repeated until the needed values in all x_i are determined. The relation for backward substitution is

$$x_N = \frac{r_N}{f_N}, \quad (20)$$

$$x_{N-1} = \frac{r_{N-1} - g_{N-1}x_N}{f_{N-1}}. \quad (21)$$

This mathematical model using the central difference scheme, splitting by coordinates and time-marching approach with the implicit treatment of unknowns has been implemented into the numerical code. In the following section, the calculations carried out based the presented mathematical model will be described and discussed.

4 CALCULATION OF TEMPERATURE DISTRIBUTION

4.1 Parameters used in the model

Numerical analysis is carried out for a 2D cross-section of amorphous Si (a-Si) strips located on a SiO₂ substrate (Fig. 1). The upper part of the computational domain is occupied by a-Si of the width 2.1 μm and thickness 0.4 μm. The substrate below the a-Si strip is considered to be infinitely wide and infinitely thick. The physical and optical parameters which are used in the model are summarized by Tables 1–3. Discretization of the computational domain is realized by a uniform grid with steps $\Delta x = 10$ nm and $\Delta z = 1$ nm. The reason for the finer mesh in z direction is in the light attenuation by Si, which follows the exponential Beer-Lambert law, giving the absorption depth of the order of only 30 nm.

The simulations were performed for cw laser with the wavelength of 488 nm, power 0.2 W and beam diameter 4.7 μm in the focus. In our simulations, laser is not moving along the strip and, thus, its intensity does not change. Figures 3 and 4 show the examples of the temperature and phase maps obtained by the model for these conditions. They correspond to the beginning stage of melting of a-Si strip (Fig. 3) and its complete melting (Fig. 4).

4.2 Effect of the size of time step

As discussed in section 2.2, the size of the time step is not critical for stability but it influences accuracy due to linear dependence of truncation error on Δt . To study this effect in our case, several values of Δt were used to model the temperature distribution during the time interval of $t = 100$ ns while keeping other parameters the same. Figure 2 presents the temperature evolution at three points on the axis of symmetry of the system cross-section.

It is seen that increasing the step 100 times does not affect the solution significantly in the most points of a-Si volume but leads to a noticeable difference in the temperature at the interface with substrate. This indicates that mainly the cells in the vicinity of an abrupt change of conductivity are sensitive to the value of Δt and this can be a potential source of error. At the time moment $t = 100$ ns, the temperature value obtained with $\Delta t = 1 \times 10^{-12}$ s is by 48 K smaller than when using $\Delta t = 1 \times 10^{-10}$ s.

Property	Value
Density of a-Si (kg/m ³)	2200
Density of l-Si (kg/m ³)	2520
Melting point of a-Si (K)	1420
Latent heat of fusion (J/kg)	1.32×10^6
Thermal conductivity in a-Si (W/m K)	1.8
Thermal conductivity in l-Si (W/m K)	$50.28 + 0.02933 (T - T_m)$
Specific heat (J/kg K)	$695.54 \exp(2.37 \times 10^{-4} T) - 8.0029 + 0.1017 \times T$

Table 1. Properties of a-Si and liquid silicon (l-Si) [Bovatssek 2010].

Property	Value	Source
Density (kg/m ³)	2200	[Bovatssek 2010]
Annealing temperature (K)	1413	[Wikipedia contributors 2019]
Melting temperature (K)	1873	[Bovatssek 2010]
Thermal conductivity (W/m K)	$T \leq 1170$ K: $1.0056 + 0.0013 \times T$ $T \geq 1170$ K: 2.514	[Bovatssek 2010]
Specific heat (J/kg K)	$708.11 + 0.29917 \times T$	[Bovatssek 2010]

Table 2. Properties of SiO₂.

Property	Value	Source
Reflection coefficient in a-Si	0.43	[Palik 1998]
Reflection coefficient in liquid state (l-Si)	0.68	[Fuchs 2000]
Absorption coefficient of a-Si (1/m)	3.2461×10^7	[Palik 1998]
Absorption coefficient of l-Si (1/m)	11.75031×10^7	[Fuchs 2000]

Table 3. Optical properties of Si at laser wavelength 488 nm.

On the other hand, the values of Δt between 1×10^{-12} s and 5×10^{-11} s give the difference in temperature at the time moment of $t = 100$ ns of only several Kelvins, leaving some space for optimization of the computational time and, at the same time, maintaining a good accuracy.

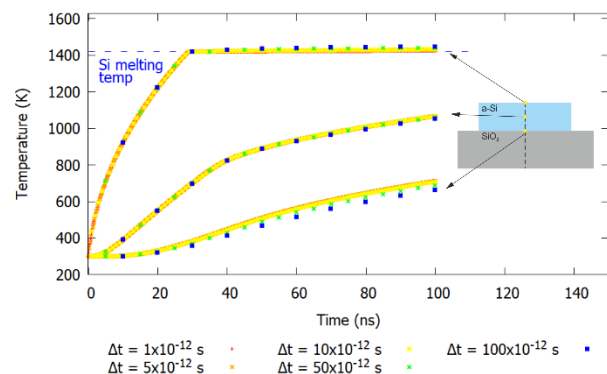


Figure 2. Evolution of the temperature at three different points in the a-Si strip cross-section calculated with the different time steps.

Based on the truncation error analysis, for further simulations we have chosen the value of time step $\Delta t=5 \times 10^{-12}$ s. In section 2.2, we mentioned that the particular implementation is energy conservative. This is illustrated in Fig. 3 where the energy balance is shown. We see that after the time $t=50$ ns, the difference between energy U_L delivered by the laser and internal energy of the material U_{Si} starts to grow with the rate of $\sim 0.1\%$ per 50 ns. This is the point where all upper surface cells of the strip reach the melting point. This rate does not increase further with time, therefore we assume that this error is probably related to the size of the melting front. By the complete melting at 600 nm, the error is still below 1%.

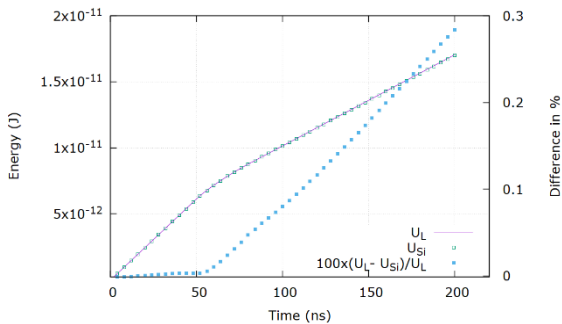


Figure 3. Balance between energy supplied by the laser U_L and rise of the internal energy U_{Si} stored in the Si computational domain. The difference between the total energies is shown in percent to quantify the energy conservation of the model.

4.3 Results of simulation of complete melting and discussion

The goal of material processing of a-Si structure is to change its phase from amorphous to polycrystalline. Large microcrystals are desirable as the boundaries of individual crystallites introduce losses and reduce the overall quality of a potential optoelectronic structure [Nickel 2003]. Numerical simulations of the temperature distribution and the dynamics of melting may be a useful study that can help to get insight into conditions prior crystallization, which starts when the laser beam moves away. As the initial step of such study, our model can be used to describe melting of the Si structure and to give information of the total time necessary to melt it through. An advantage of laser processing of such combination of materials is in the fact that a non-absorbing material (fused silica glass, SiO_2 , in our case) should be much less affected by the heat and therefore its original properties are kept except for some heat-affected area. The size of this affected can also be determined by this model.

When irradiation is started ($t = 0$ ns), the surface layer undergoes rapid heating so that melting starts already at ~ 30 ns. As consumption of the latent heat of fusion takes time, a nano-sized region exists where the temperature has reached the melting point but the material in this region is not still completely molten. From Fig. 4, bottom, it is seen that the thickness of this layer (highlighted by green) is only few nanometers.

The time required for complete melting was found to be almost exactly 600 ns (Fig. 5). To this time moment, overheating of the SiO_2 substrate above the annealing temperature ($\sim 1413\text{K}$ [Wikipedia contributors 2019]) is reached at a depth of only few nanometers. Thus, the substrate does not experience noticeable softening and corresponding damage due compaction of fused silica matrix [Sakakura 2011] that can be important for optical applications. At longer laser-exposure times, glass compaction

under the Si strip may influence the waveguiding quality as mentioned above.

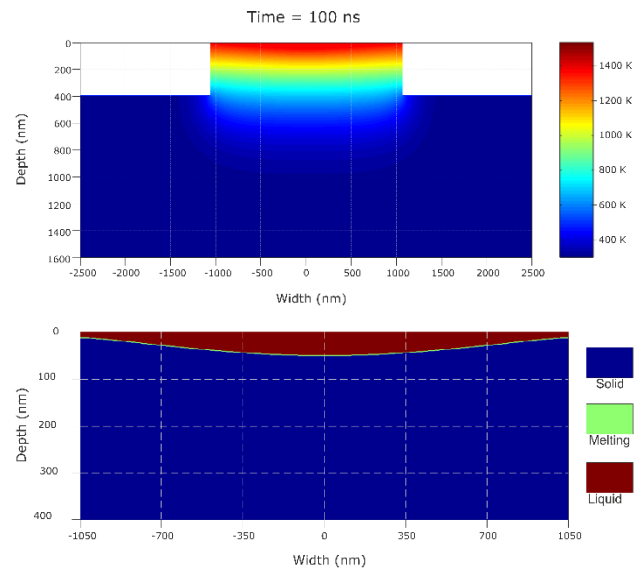


Figure 4. Temperature map of complete cross-section of a-Si/ SiO_2 system (top) and the phase map showing the position of the melting front in a-Si (bottom). The time moment is 100 ns from the beginning of irradiation.

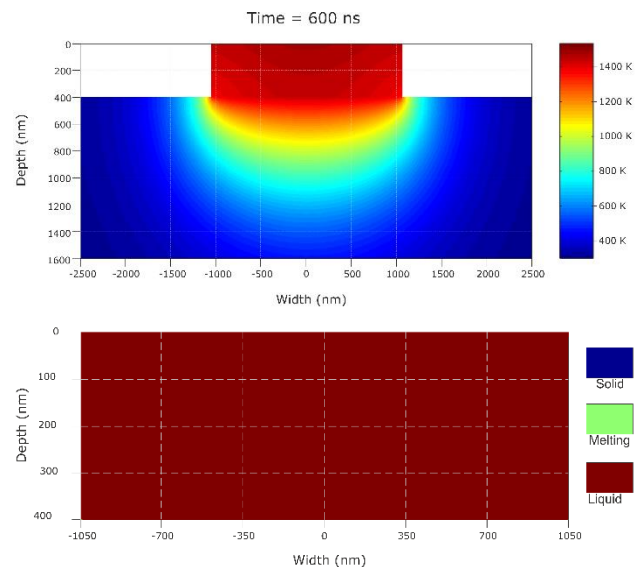


Figure 5. The same as in Fig. 3 for the time moment 600 ns.

Simulations also reveal the correlation between the phase change undergone in the a-Si strip and heating of the substrate. The rate of heating is always accelerated with melting within a-Si strip but is lowered for the substrate when the time of complete melting of Si is reached. This can be attributed to the increased conductivity in the liquid phase of silicon that leads to faster smoothing of temperature gradients in the molten region.

Total time of melting of a-Si strip is in a good agreement with the previous work for the fibre geometry, where the a-Si cross-section was circular and surrounded by the SiO_2 cladding [Healy 2014].

5 CONCLUSIONS

The 2D numerical model solving the heat flow equation for the case of absorbing material on a transparent substrate irradiated by a continuous laser has been presented. It is proven that the

implementation is consistent, stable and represents a well-posed problem.

Our simulations predict the total time necessary for complete melting. For the experimental conditions when cw Ar+ laser with the power of 0.2 W is used for the beam diameter 4.7 μm , the melting time is ~ 600 ns. Depth of softening of SiO₂ substrate, where the temperature reaches annealing point, was found to be negligibly small to this time.

A weak point of these simulations is an overestimation of the temperature for the cells close to high temperature gradients. To avoid overestimation, the time steps has to be decreased to 1×10^{-10} s or even smaller. There is also a limit in respect of simulations of long exposure times, when material evaporation can start as well as cooling/solidification must proceed with formation of nano-/microcrystallites, that calls for further improvement of the model.

ACKNOWLEDGMENTS

This work was supported by the European Regional Development Fund and the state budget of the Czech Republic (Project No. BIATRI: CZ.02.1.01/0.0/0.0/15_003/0000445), the Ministry of Education, Youth and Sports of the Czech Republic (Programmes NPU I Project No. LO1602, and the Large Research Infrastructure Project No. LM2015086). J.B. also acknowledges the support of the Grant Agency of the Czech Technical University in Prague (No. SGS16/244/OHK4/3T/14). The authors are grateful to Prof. A.C. Peacock for involving in this research and valuable discussions.

REFERENCES

- [Bovatssek 2010] Bovatssek, J., et al. Thin film removal mechanisms in ns-laser processing of photovoltaic materials. *Thin Solid Films*, 2010, Vol. 518, pp 2897-2904.
- [Bulgakova 2010] Bulgakova, O.A., et al. A model of nanosecond laser ablation of compound semiconductors accounting for non-congruent vaporization. *Appl. Phys. A*, 2010, Vol. 101, pp 53–59.
- [Courant 1967] Courant, R, et al. Über die partiellen Differenzengleichungen der Mathematischen Physik. *Math. Ann.*, 1928, Vol. 100, pp 32-74. (English translation, with commentaries by Lax PB, Widlund OB, Parter, SV, in *IBM J Res Develop* 11 (1967).)
- [Franz 2019] Franz, Y., et al. Laser crystallized low-loss polycrystalline silicon waveguides, *Opt. Express*, 2019, Vol. 27, pp 4462-4470.

[Fuchs 2000] Fuchs, M., Optical properties of liquid silicon: the integral equation approach. *J. Phys.: Condens. Matter*, 2000, Vol. 12, pp 4341-4351.

[Godunov 1987] Godunov, S. K. and Ryabenkii, V. S. *Difference schemes*, Elsevier Science Publishers B.V., 1987, ISBN-13: 0444702334.

[Healy 2014] Healy, N., et al., Extreme electronic bandgap modification in laser-crystallized silicon optical fibres. *Nat. Mater.*, 2014, Vol. 13, p.1122-1127.

[Hoffman 2001] Hoffman, J. D., *Numerical Methods for Engineers and Scientists*, CRC Press, 2001, ISBN: 9780824704438.

[Mazumder 2015] Mazumder, S. *Numerical Methods for Partial Differential Equations*, Academic Press, 2015, ISBN: 9780128498941.

[Nickel 2003] Nickel, N. *Laser Crystallization of Silicon - Fundamentals to Devices*, Academic Press, 2003, ISBN: 9780127521848.

[Palik 2003] E.D. Palik (Ed.), *Handbook of Optical Constants of Solids*, Academic Press, Orlando FL, 1998. ISBN: 9780125444156.

[Sakakura 2011] M. Sakakura, M., et al. Thermal and shock induced modification inside a silica glass by focused femtosecond laser pulse. *J. Appl. Phys.*, 2011, Vol. 109, Article 023503.

[Wikipedia contributors 2019] Wikipedia contributors. Fused quartz. *Wikipedia, The Free Encyclopedia*, 2019, Aug 2, 21:25 UTC [cited 2019 Sep 3] 2019, Available from: https://en.wikipedia.org/w/index.php?title=Fused_quartz&oldid=909069037

[Zhvavyi 2006] Zhvavyi, S.P. and Zykov, G.L. Simulation of dynamics of phase transitions in CdTe by pulsed laser irradiation. *Appl. Surf. Sci.*, 2006, Vol. 253, pp. 586-591.

CONTACTS:

Ing. Jiri Beranek
Prof. Nadezhda Bulgakova, Dr.Sc.
HiLASE Centre, Institute of Physics of the Czech Academy of Sciences, Za Radnicí 828, 252 41, Dolní Břežany
+420 314 007 735, jiri.beranek@hilase.cz, www.hilase.cz